Check for updates

A Journal of the Gesellschaft Deutscher Chemiker

Angewandte International Edition GDCh Chemie

www.angewandte.org

## Accepted Article

**Title:** Controllable Cu0-Cu+ Sites for Electrocatalytic Reduction of Carbon Dioxide

**Authors:** Jinlong Gong

This manuscript has been accepted after peer review and appears as an Accepted Article online prior to editing, proofing, and formal publication of the final Version of Record (VoR). This work is currently citable by using the Digital Object Identifier (DOI) given below. The VoR will be published online in Early View as soon as possible and may be different to this Accepted Article as a result of editing. Readers should obtain the VoR from the journal website shown below when it is published to ensure accuracy of information. The authors are responsible for the content of this Accepted Article.

**To be cited as:** *Angew. Chem. Int. Ed.* 10.1002/anie.202105118

**Link to VoR:** https://doi.org/10.1002/anie.202105118

WILEY-VCH

10.1002/anie.202105118

COMMUNICATION

WILEY-VCH

# Controllable $Cu^0$-$Cu^+$ Sites for Electrocatalytic Reduction of Carbon Dioxide

Xintong Yuan, Sai Chen, Dongfang Cheng, Lulu Li, Wenjin Zhu, Dazhong Zhong, Zhi-Jian Zhao, Jingkun Li, Tuo Wang, and Jinlong Gong*[a]

**Abstract:** Cu-based electrocatalysts can effectively facilitate carbon dioxide electrochemical reduction ($CO_2$ER) to produce multi-carbon products. However, the roles of $Cu^0$ and $Cu^+$ and the mechanistic understanding remain elusive. This paper describes the controllable construction of $Cu^0$-$Cu^+$ sites derived from the well-dispersed cupric oxide supported on copper phyllosilicate lamella to enhance $CO_2$ER performance. Specifically, 20% Cu/$CuSiO_3$ shows the superior $CO_2$ER performance with 51.8% $C_2H_4$ Faraday efficiency at -1.1 V vs reversible hydrogen electrode (RHE) during the 6 hours-test. *In situ* attenuated total reflection infrared spectra and density functional theory calculations were employed to elucidate the reaction mechanism over $Cu^0$-$Cu^+$ sites. The enhancement in $CO_2$ER activity is mainly attributed to the synergistic effect of $Cu^0$-$Cu^+$ pairs: The $Cu^0$ site activates $CO_2$ and facilitates the following electron transfers; while the $Cu^+$ site strengthens the *CO adsorption to further boost C-C coupling. This paper provides an efficient strategy to rationally design Cu-based catalysts with viable valence states to boost $CO_2$ER.

Electrocatalytic $CO_2$ reduction ($CO_2$ER) is of great significance to complete the carbon cycle and solve the energy and environmental crisis.[1] Particularly, Cu-based catalysts are of great interest for $CO_2$ER since Cu is in favor of binding *CO intermediate and converting it into multi-carbon products. Specially, oxide-derived Cu (OD-Cu) catalyst[2] has been widely studied due to its excellent $CO_2$ER performance towards valuable multi-carbon products.[3] Electronic structures[3c, 4] and geometric structures[2b, 5] have been extensively studied to increase the reactivity. Nevertheless, the reaction mechanism and real active site of OD-Cu are still unclear, mainly due to that copper oxide is reduced rapidly during the reduction process and then reoxidized rapidly once the applied potential is stopped. Recently, studies show that $Cu^0$ is the active site toward $CO_2$ER, since $Cu^+$ cannot be stably present in OD-Cu during the electroreduction process.[6]

However, in both electrocatalysis and traditional catalysis, *CO is more strongly adsorbed over $Cu^+$ than $Cu^0$,[4a, 4b, 7] which solves the vital dynamics problem in $CO_2$ER, i.e., enhancing adsorption of *CO to facilitate *CO-*CO dimerization. Hence, it is extremely meaningful to stabilize $Cu^+$ for enhancing the selectivity of multi-carbon products. Numerous studies have been carried out to stabilize $Cu^+$ and improve $CO_2$ER performance. For example, $N_3^-$ in the perovskite-type $Cu_3N$ structure is reported to stabilize $Cu^+$, and the $Cu^+$ plays the key role for converting $CO_2$ to $C_2H_4$ with Faraday efficiency (FE) of 60% at -1.6 vs reversible hydrogen electrode (RHE).[8] Additionally, the copper oxychloride sol-gel material shows sluggish reduction kinetics of copper and stabilized $Cu^+$, leading to a FE of 54% for $C_2H_4$ and $C_2H_5OH$ ($C_2$) at -1.2 V vs RHE.[4a] However, $Cu^+$ alone cannot guarantee excellent $CO_2$ER performance. $CO_2$ is a thermodynamically stable molecular with a standard formation enthalpy of -393.5 kJ $mol^{-1}$.[9] Thus, another essential thermodynamic problem, i.e., how to reduce the energy barrier of $CO_2$ activation, need to be resolved during $CO_2$ER.[10] According to density function theory (DFT) calculations, $CO_2$ activation and CO dimerization comes from the synergism between active $Cu^0$ and $Cu^+$ sites.[11]

This paper designs the catalysts with tunable $Cu^+$ and $Cu^0$ pairs, and elucidates their individual and synergic roles via *in situ* experiments and DFT calculations. We synthesized cupric oxide particles supported on copper phyllosilicate lamella (CuO/$CuSiO_3$) via ammonia evaporation hydrothermal method (AEM). During the initial electroreduction process, $Cu^{2+}$ sites in CuO/$CuSiO_3$ are reduced to $Cu^0$ and $Cu^+$ sites (Cu/$CuSiO_3$). $Cu^0$ promotes the activation of $CO_2$ by reducing the thermodynamic activation barrier, while $Cu^+$ enhances *CO adsorption, and thus the kinetics of C-C coupling. The $Cu^+$ species stably exist as efficient active sites to increase $CO_2$ER activity as evidenced by *in situ* infrared spectroscopy. By adjusting the Cu loading, the ratio of $Cu^0$-$Cu^+$ is controlled to further regulate the binding energy of reaction intermediates. Particularly, 20% Cu/$CuSiO_3$ shows a FE (-1.1 V vs RHE) of 51.8% and 82% toward $C_2H_4$ and carbonaceous products ($C_1$+$C_2$), respectively. This is among the competitive $CO_2$ER performances over Cu-based catalysts for $C_2H_4$ production in H-cell (Table S1).

The copper phyllosilicate lamella can boost the well-dispersion of CuO particles and enhance metal-support interaction markedly, which originates from its characteristic preparation method. By adding ammonium hydroxide to adjust pH, $\equiv SiOCu^{II}$ monomer is formed via the reaction of the silanol groups with the $Cu^{2+}$ complex through hydrolytic adsorption.[12] Then the target structure is obtained by hydrothermal polymerization and calcination (Figure 1a). The copper phyllosilicate and copper hydroxide could be discriminated by Fourier transform infrared for their structural OH groups (Figure S1). For the sample before calcination, the peaks appearing at 937 and 690 $cm^{-1}$ are attribute to $\delta_{OH}$ bands from $Cu(OH)_2$.[13] The appearance of $\nu_{SiO}$ shoulder at 1040 $cm^{-1}$ and $\delta_{OH}$ vibration at 670 $cm^{-1}$ arises from copper phyllosilicate,[14] suggesting the complete decomposition of $Cu(OH)_2$ to CuO and the existence of copper phyllosilicate in CuO/$CuSiO_3$. With the increasing amount of Cu precursor, the amount of copper silicate reaches the maximum and the amount of CuO gradually increases, thus adjusting the ratio of $Cu^0$ and $Cu^+$. 20% CuO/$CuSiO_3$ means the mass feed ratio of copper precursor is 20%, and the like. There is a ~3-4 nm layer of well-dispersed CuO particles supported on the copper phyllosilicate lamella in 20% CuO/$CuSiO_3$ (Figure 1b-c). The elemental mapping images (Figure 1d) highlight the existance of CuO particles and display the uniform dispersion of Cu, Si and O in $CuSiO_3$. The Cu $2p_{3/2}$ peaks at ~933.1-935.8 eV and 2p→3d

[a] X. Yuan, S. Chen, D. Cheng, L. Li, W. Zhu, D. Zhong, Prof. Dr. Z. J. Zhao, Prof. Dr. J. Li, Prof. Dr. J. Gong
Key Laboratory for Green Chemical Technology of Ministry of Education, School of Chemical Engineering and Technology, Collaborative Innovation Center of Chemical Science and Engineering
Tianjin University
Weijin Road 92, Tianjin, 300072 (China)
E-mail:jlgong@tju.edu.cn

Supporting information for this article is given via a link at the end of the document.

Accepted Manuscript

This article is protected by copyright. All rights reserved.

10.1002/anie.202105118


WILEY-VCH

satellite peak at ~943.9 eV in X-ray photoelectron spectroscopy (XPS) indicate the existence of $Cu^{2+}$ with a d9 electron configuration in 20% CuO/$CuSiO_3$ (Figure 1e). The asymmetry of the Cu $2p_{3/2}$ binding energy values (~935.8 and ~933.1 eV) shows the existence of two different $Cu^{2+}$, ascribing to copper phyllosilicate and CuO.[14a] Because of the amorphous structure of copper silicate, X-ray diffraction (XRD) patterns only demonstrate weak peaks of $SiO_2$ and CuO (Figure S2).[12] It's clear that as the Cu loading increases, the peaks of CuO gradually become more obvious, indicating there are more CuO particles.

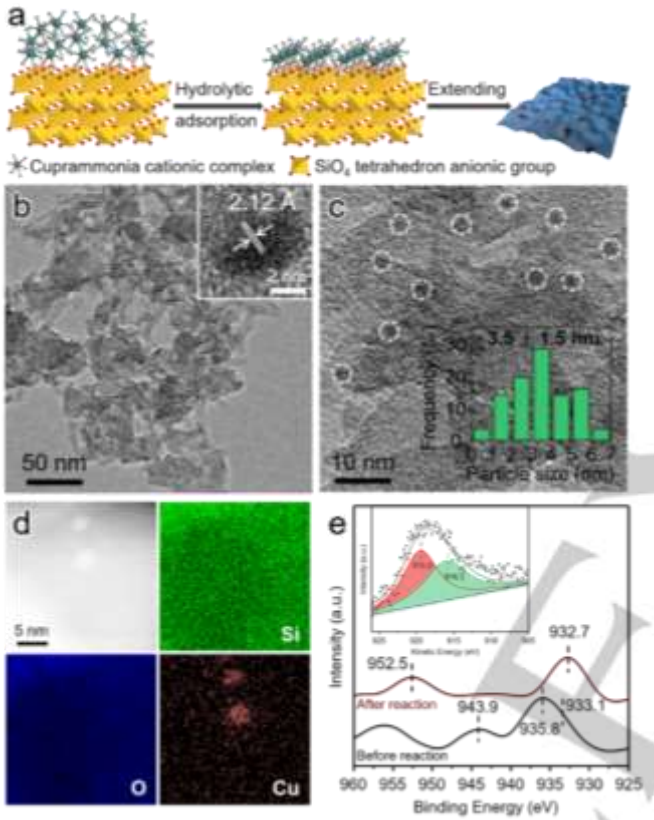


**Figure 1.** (a) Schematic illustration of the synthetic process, (b-c) transmission electron microscopy (TEM) image, (d) elemental mapping, and (e) Cu 2p XPS spectra of 20% CuO/$CuSiO_3$. The inset in (e) shows Cu LMM XEAS spectrum of 20% Cu/$CuSiO_3$ after 6 h reaction.

To explore the origin of $CO_2$ER reactivity, catalytic performances over Cu/$CuSiO_3$ with different loadings were further investigated (Figure 2a, S3). All catalysts exhibit a structure of copper phyllosilicate lamella with well-dispersed CuO particles (Figure S4), eliminating the influence of morphology on $CO_2$ER activity. Particularly, 20% Cu/$CuSiO_3$ demonstrates a notably enhanced catalytic activity, i.e., 51.8% $C_2H_4$ FE and 82% $C_1$+$C_2$ FE at -1.1 V vs RHE, which is stable during the 6 h reaction (Figure 2a-b). According to the change of lattice spacing, surface CuO particles are reduced to $Cu^0$ particles and the support still keeps the uniform dispersion of Cu, O and Si (Figure 2c, d) after 6 h reaction. Also, the Cu 2p peak around 943.9 eV disappeared and two overlapping peaks appeared at 919.0 and 916.2 eV in Cu LMM X-ray Excited Auger spectroscopy (XEAS), indicating the maintenance of $Cu^0$ and $Cu^+$ (Figure 1e). The strong interaction between Cu ions and $SiO_2$ prepared by AEM method[12] can supply stable $Cu^0$ and $Cu^+$ and remain intact even after intense electrochemical process, thus, guaranteeing the superior $CO_2$ER performance. Besides, linear sweeping voltammetry (LSV) (Figure 2e) and electrochemical impedance spectroscopy (Figure S5) demonstrates the preferable catalytic performance and charge transfer resistance of 20% Cu/$CuSiO_3$.

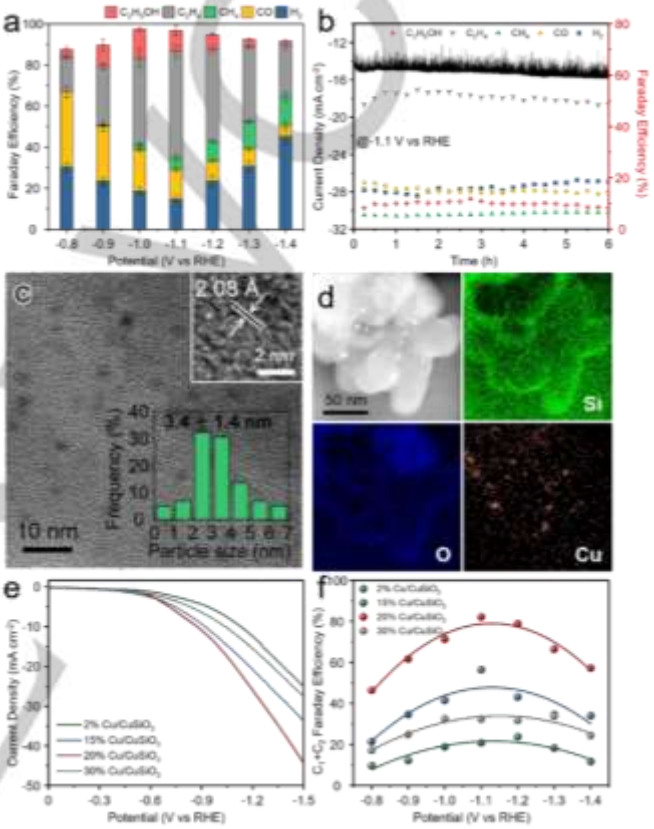


**Figure 2.** (a) FE and (b) stability test of 20% Cu/$CuSiO_3$. (c) TEM image and (d) elemental mapping of 20% Cu/$CuSiO_3$ after 6 h reaction. (e) LSV and (f) the best $C_1$+$C_2$ FE of different loadings of Cu/$CuSiO_3$.

*In situ* attenuated total reflection infrared (ATR-IR) spectroscopy is employed to investigate the adsorbed CO at conditions closely mimicking real reaction environments. The 20% Cu/$CuSiO_3$ shows two stretching bands of linear-bonded *CO in the 2040-2100 $cm^{-1}$ range[15] (Figure 3a), which are attributed to CO adsorption on $Cu^+$ and $Cu^0$ sites.[16] This phenomenon could not be attributed to surface reconstruction since there is no such phenomenon in Ar-saturated 0.1 M $KHCO_3$ solution (Figure S6). Besides, the low frequency band gradually increases with the increase of applied potential, which is not consistent with previous studies.[17] Simultaneously, DFT calculations (Figure S7) predict the frequency of CO over $Cu^+$ and $Cu^0$ is 2115 $cm^{-1}$ and 2023 $cm^{-1}$, respectively, agreeing well with the *in situ* ATR-IR results taking into consideration of the error of simulation and the peak shifts due to Stark effect.[18] *In situ* ATR-

Accepted Manuscript

This article is protected by copyright. All rights reserved.

IR spectra of $Cu/CuSiO_3$ with different loadings (Figure 3b, S8) demonstrate that the proportion of $Cu^0$ increases gradually with the increase of Cu loading, which is consistent with the XRD trend. Thus, the proper proportion of $Cu^0$-$Cu^+$ sites in 20% $Cu/CuSiO_3$ is the key to obtain superior $CO_2$ER performance. As the potential increases, the proportion of $Cu^0$ gradually increases, indicating that more $Cu^+$ is reduced to $Cu^0$ with the higher reduction energy input. However, even if the stability of $Cu^+$ is relatively different under different potentials, $Cu^+$ remains stable at 10% at -1.1 V vs RHE for 60 min (Figure S9, Table S3). This demonstrates the stable existence of $Cu^+$ that is responsible for the excellent $CO_2$ER performance at -1.1 V vs RHE (Figure 3a). Of course, the reconstruction of Cu is inevitable under the fierce electrochemical environment. The defective sites and roughened morphology produced therein may also lead to significantly enhanced performance, which will require more investigation with careful *in situ* measurements further.[19]

The catalytic performance of $Cu/CuSiO_3$ with different Cu loadings was investigated to explore the roles of $Cu^0$ and $Cu^+$ in $CO_2$ER. Serious hydrogen evolution reaction (HER) occurs for 2% $Cu/CuSiO_3$ (Figure S3a) with ~40% Cu species exist as $Cu^+$ in copper phyllosilicate. As Cu loading increases to 20%, the proportion of $Cu^0$ increases gradually, and the $C_1$+$C_2$ FE of $CO_2$ER reaction increases from 24.9% to 84.9% (Figure 2a, S3). Thus, the increase of $Cu^0$ gradually turns on $CO_2$ER reaction, and 20% $Cu/CuSiO_3$ exhibits the best $CO_2$ER performance (Figure 2f, S10). This suggests that $CO_2$ is activated over $Cu^0$, which initiates the $CO_2$ER reaction. This agrees well with the results from Goddard et al.[11] As the Cu loading increase to 30%, $C_2H_4$ FE declines and the overpotential of $C_2H_4$ production increases (Figure S3c) because there is almost no enough $Cu^+$ to promote C-C coupling. Then we correlate $Cu^0/(Cu^0+Cu^+)$ from *in situ* ATR-IR (Table S2) with $CO_2$ER performance. The $C_2H_4$ FE and $C_1$+$C_2$ FE show volcano trends as the ratio of $Cu^0$ increases (Figure 3c, d), indicating a strong dependence of $CO_2$ER activity on the ratio of $Cu^0$-$Cu^+$ and unbalanced ratio of $Cu^0$-$Cu^+$ can cause serious HER. Particularly, the volcano peaks reach the maximum when the proportion of $Cu^0$ accounts for ~86%. Furthermore, the proportion of CO in $C_1$+$C_2$ is higher with increasing $Cu^0$ ratio (Figure 3e), which suggests $Cu^0$ improves the selectivity of CO. Thus, it is inferred that $Cu^0$ initially activates $CO_2$, while $Cu^+$ enhances *CO adsorption to promote subsequent *CO-*CO dimerization.

DFT calculations were further conducted to elucidate the mechanism over $Cu^0$-$Cu^+$ sites. According to XPS results[10a] (Figure S11) and previous work,[12] 20% $Cu/CuSiO_3$ were rich in surface hydroxyl, thus we adjusted the number of hydroxyls to modify the valence of Cu (Figure 4b). *CO is an important intermediate of $CO_2$ER to multi-carbon products as the reaction pathways for CO and $C_2H_4$ deviate at the adsorbed *CO intermediate.[4a] Desorption of *CO leads to the formation of CO, while dimerization of two *CO leads to the formation of $C_2$.[20] For the goal of producing multi-carbon products, it's necessary to establish enough *CO coverage to favor the kinetics of C-C coupling (Figure 4a). Adsorption energy of *CO on $Cu^0$, $Cu^+$ and $Cu^0$-$Cu^+$ sites (Figure 4c) indicate $Cu^0$-$Cu^+$ and $Cu^+$ sites have relatively stronger *CO adsorption energy than $Cu^0$ sites, which enhances the *CO coverage and promotes the subsequent *CO-*CO dimerization.[4b] Furthermore, we calculated the formation energy of *COCOH, the key intermediate in the $C_2$ pathway, as the descriptor of the $C_2$ activity,[21] and discovered that $Cu^0$ as well as $Cu^0$-$Cu^+$ sites are favorable in forming the *COCOH, leading to the formation of $C_2$ rather than CO. However, the $C_2$ activity over $Cu^0$ sites is hindered by the low *CO coverage due to weak *CO adsorption. Thus, $Cu^0$-$Cu^+$ sites with sufficient *CO coverage and relatively low *COCOH formation energy is most preferable for C-C coupling and the further production of $C_2$.

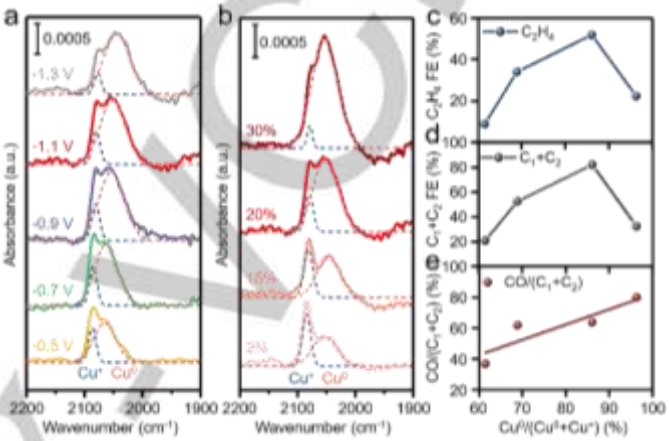


**Figure 3.** *In situ* ATR-IR of (a) 20% $Cu/CuSiO_3$ at different potentials, and (b) $Cu/CuSiO_3$ with different loadings at -1.1 V vs. RHE. The correlation of (c) $C_2H_4$ FE, (d) $C_1$+$C_2$ FE and (e) $CO/(C_1+C_2)$ with $Cu^0/(Cu^0+Cu^+)$.

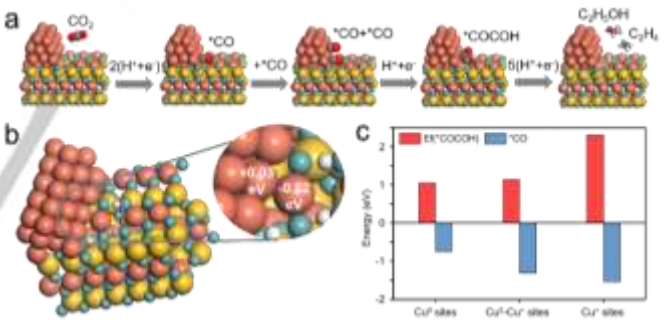


**Figure 4.** (a) Proposed pathway for *CO-*CO dimerization to $C_2$, (b) optimized model representing $Cu^0$-$Cu^+$ sites and inset shows Bader charge for $Cu^0$-$Cu^+$ sites, (c) the formation energy of *COCOH and adsorption energy of *CO on $Cu^0$, $Cu^+$ and $Cu^0$-$Cu^+$ sites.

In summary, we design copper phyllosilicate lamella with well-dispersed CuO particles which could be reduced to $Cu^+$ and $Cu^0$ sites. Controllable $Cu^+$-$Cu^0$ sites is obtained by synthesizing a series of $CuO/CuSiO_3$ with different Cu loadings. A notably enhancement in the $CO_2$ER activity is observed on 20% $Cu/CuSiO_3$, achieving a $C_2H_4$ FE of 51.8% and a $C_1$+$C_2$ FE of 82%, as well as stability up to 6 h at -1.1 V vs RHE. *In situ* ATR-IR and DFT calculations elucidates the roles of $Cu^0$ and $Cu^+$: the former initiates the $CO_2$ activation, while the latter strengthens the *CO adsorption and promotes C-C coupling. This synergistic effect of $Cu^0$ and $Cu^+$ breaks the thermodynamic and kinetic limitations of $CO_2$ER. This work offers a novel strategy to the rational design of

Accepted Manuscript

This article is protected by copyright. All rights reserved.

Cu-based catalysts to boost $CO_2$ER. However, this paper failed to elucidate the distribution of $Cu^0$ and $Cu^+$ in the $Cu/CuSiO_3$. By the aid of more advanced in situ technology to explore and clarity the CO2ER reaction mechanism is one of the future research directions.

**Acknowledgements**

We acknowledge the National Key Research and Development Program of China (2016YFB0600901), the National Science Foundation of China (21525626, 22038009, 51861125104), and the Program of Introducing Talents of Discipline to Universities (BP0618007) for financial support.

**Keywords:** $CO_2$ electrochemical reduction, $Cu^0$-$Cu^+$ pairs, $CO_2$ activation, C-C coupling, synergistic effect

**References**

[1] a) L. Zhang, Z. J. Zhao, J. Gong, *Angew. Chem. Int. Ed.* **2017**, 56, 11326-11353; b) R. Xu, H. Xu, S. Ning, Q. Zhang, Z. Yang, J. Ye, *Trans. Tianjin Univ.* **2020**, *26*, 470-478; c) S. Wu, J. Wang, Q. Li, Z. Huang, Z. Rao, Y. Zhou, *Trans. Tianjin Univ.* **2021**, *27*, 155-164.

[2] a) C. W. Li, J. Ciston, M. W. Kanan, Nature 2014, 508, 504-507; b) C. W. Li, M. W. Kanan, *J. Am. Chem. Soc.* **2012**, 134, 7231-7234.

[3] a) Y. Lum, J. W. Ager, *Nat. Catal.* **2019**, 2, 86–93; b) C. S. Chen, J. H. Wan, B. S. Yeo, *J. Phys. Chem. C* **2015**, 119, 26875-26882; c) H. Mistry, A. S. Varela, C. S. Bonifacio, I. Zegkinoglou, I. Sinev, Y.-W. Choi, K. Kisslinger, E. A. Stach, J. C. Yang, P. Strasser, B. R. Cuenya, *Nat. Commun.* **2016**, 7, 12123; d) Y. Ling, Q. Ma, Y. Yu, B. Zhang, *Trans. Tianjin Univ.* **2021**. DOI: 10.1007/s12209-021-00283-x

[4] a) P. De Luna, R. Quintero-Bermudez, C.-T. Dinh, M. B. Ross, O. S. Bushuyev, P. Todorović, T. Regier, S. O. Kelley, P. Yang, E. H. Sargent, *Nat. Catal.* **2018**, 1, 103-110; b) Y. Zhou, F. Che, M. Liu, C. Zou, Z. Liang, P. De Luna, H. Yuan, J. Li, Z. Wang, H. Xie, H. Li, P. Chen, E. Bladt, R. Quintero-Bermudez, T. K. Sham, S. Bals, J. Hofkens, D. Sinton, G. Chen, E. H. Sargent, *Nat. Chem.* **2018**, 10, 974-980; c) Y. Lum, J. W. Ager, *Angew. Chem. Int. Ed.* **2018**, 57, 551-554.

[5] a) W. Luo, X. Nie, M. J. Janik, A. Asthagiri, *ACS Catal.* **2016**, 6, 219-229; b) C. Choi, T. Cheng, M. Flores Espinosa, H. Fei, X. Duan, W. A. Goddard III, Y. Huang, *Adv. Mater.* **2018**, 31, 1805405.

[6] a) S. Nitopi, E. Bertheussen, S. B. Scott, X. Liu, A. K. Engstfeld, S. Horch, B. Seger, I. E. L. Stephens, K. Chan, C. Hahn, J. K. Norskov, T. F. Jaramillo, I. Chorkendorff, *Chem. Rev.* **2019**, 119, 7610-7672; b) A. D. Handoko, K. W. Chan, B. S. Yeo, *ACS Energy Lett.* **2017**, 2, 2103-2109.

[7] K. Hadjiivanov, H. Knözinger, *Phys. Chem. Chem. Phys.* **2001**, 3, 1132-1137.

[8] Z. Yin, C. Yu, Z. Zhao, X. Guo, M. Shen, N. Li, M. Muzzio, J. Li, H. Liu, H. Lin, J. Yin, G. Lu, D. Su, S. Sun, *Nano Lett.* **2019**, 19, 8658-8663.

[9] H. Dong, L. Zhang, L. Li, W. Deng, C. Hu, Z. J. Zhao, J. Gong, *Small* **2019**, 15, e1900289.

[10] a) W. Zhu, R. Michalsky, O. Metin, H. Lv, S. Guo, C. J. Wright, X. Sun, A. A. Peterson, S. Sun, *J. Am. Chem. Soc.* **2013**, 135, 16833-16836; b) A. Alvarez, M. Borges, J. J. Corral-Perez, J. G. Olcina, L. Hu, D. Cornu, R. Huang, D. Stoian, A. Urakawa, *Chemphyschem* **2017**, 18, 3135-3141.

[11] H. Xiao, W. A. Goddard, 3rd, T. Cheng, Y. Liu, *Proc. Natl. Acad. Sci. U.S.A.* **2017**, 114, 6685-6688.

[12] J. Gong, H. Yue, Y. Zhao, S. Zhao, L. Zhao, J. Lv, S. Wang, X. Ma, *J. Am. Chem. Soc.* **2012**, 134, 13922-13925.

[13] F. C. Zhiwei Huang, Jingjing Xue, Jianliang Zuo, Jing Chen, and Chungu Xia, *J. Phys. Chem. C* **2010**, 114, 16104–16113.

[14] a) A. Chen, X. Yu, Y. Zhou, S. Miao, Y. Li, S. Kuld, J. Sehested, J. Liu, T. Aoki, S. Hong, M. F. Camellone, S. Fabris, J. Ning, C. Jin, C. Yang, A. Nefedov, C. Wöll, Y. Wang, W. Shen, *Nat. Catal.* **2019,** 2, 334-341; b) L. Chen, P. Guo, M. Qiao, S. Yan, H. Li, W. Shen, H. Xu, K. Fan, *J. Catal*. **2008**, 257, 172-180.

[15] H. Zhang, X. Chang, J. G. Chen, W. A. Goddard, 3rd, B. Xu, M. J. Cheng, Q. Lu, *Nat. Commun.* **2019**, 10, 3340.

[16] a) L. Wan, Q. Zhou, X. Wang, T. E. Wood, L. Wang, P. N. Duchesne, J. Guo, X. Yan, M. Xia, Y. F. Li, A. A. Jelle, U. Ulmer, J. Jia, T. Li, W. Sun, G. A. Ozin, *Nat. Catal.* **2019**, 2, 889-898; b) W. Su, S. Wang, P. Ying, Z. Feng, C. Li, *J. Catal.* **2009**, 268, 165-174.

[17] C. M. Gunathunge, X. Li, J. Li, R. P. Hicks, V. J. Ovalle, M. M. Waegele, *J. Phys. Chem. C* **2017**, 121, 12337-12344.

[18] a) X. Yuan, L. Zhang, L. Li, H. Dong, S. Chen, W. Zhu, C. Hu, W. Deng, Z. J. Zhao, J. Gong, *J. Am. Chem. Soc.* **2019**, 141, 4791-4794; b) M. M. Sartin, Z. Yu, W. Chen, F. He, Z. Sun, Y.-X. Chen, W. Huang, *J. Phys. Chem. C* **2018**, 122, 26489-26498.

[19] G. M. Tomboc, S. Choi, T. Kwon, Y. J. Hwang, K. Lee, *Adv. Mater.* **2020**, 32, e1908398.

[20] Y. Zheng, A. Vasileff, X. Zhou, Y. Jiao, M. Jaroniec, S. Z. Qiao, *J. Am. Chem. Soc.* **2019**, 141, 7646-7659.

[21] Y. Huang, Y. Chen, T. Cheng, L. W. Wang, W. A. Goddard, *ACS Energy Lett.* **2018**, 3, 2983-2988.

Accepted Manuscript

This article is protected by copyright. All rights reserved.

10.1002/anie.202105118



WILEY-VCH

# COMMUNICATION

Controllable $Cu^0$-$Cu^+$ pairs derived from the well-dispersed cupric oxide supported on copper phyllosilicate lamella can break thermodynamic and kinetic limitations of $CO_2$ reduction reaction and achieve the superior $CO_2$ electronreduction performance.

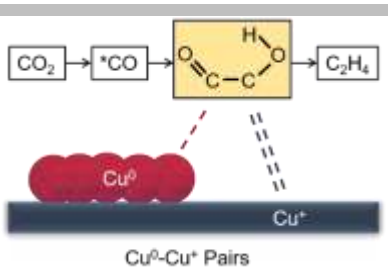


$Cu^0$-$Cu^+$ Pairs

Xintong Yuan, Sai Chen, Dongfang Cheng, Lulu Li, Wenjin Zhu, Dazhong Zhong, Zhi-Jian Zhao, Jingkun Li, Tuo Wang, and Jinlong Gong*

**Page No. – Page No.**

**Controllable $Cu^0$-$Cu^+$ Sites for Electrocatalytic Reduction of Carbon Dioxide**

WILEY-VCH

Accepted Manuscript

This article is protected by copyright. All rights reserved.